Supporting Information

Galvanic replacement reaction in perovskite oxide for superior chemiresistors

Jong Won Baek[a,†], Yoon Hwa Kim[a,b,†], Jaewan Ahn[a], Dong-Ha Kim[a,c], Hamin Shin[a], Jaehyun Ko[a], Seyeon Park[a], Chungseong Park[a], Euichul Shin[a], Ji-Soo Jang[d,], and Il-Doo Kim[a,*]*

Prof. I.-D. Kim, J. W. Baek, Dr. Y. H. Kim, Dr. J. Ahn, Dr. D.-H. Kim, H. Shin, J. Ko, S. Park, C. Park, E. Shin, M. Kim

[1]Department of Materials Science and Engineering, Korea Advanced Institute of Science and Technology (KAIST), 291 Daehak-ro, Yuseong-gu, Daejeon 34141, Republic of Korea

Dr. Y. H. Kim

[2]Forensic toxicology & chemistry, Seoul institute, National Forensic Service, 139 Jiyang-ro, Yangcheon-gu, Seoul 08036, Republic of Korea

Dr. D.-H. Kim

[3]Department of Chemistry, Massachusetts Institute of Technology, 77 Massachusetts Avenue, Cambridge, Massachusetts, 02139, United States

Dr. J.-S. Jang

[4]Electronic Materials Research Center, Korea Institute of Science and Technology, Seoul 02792, Republic of Korea

[†]These authors contributed equally

*Correspondence should be addressed to wkdwltn92@kist.re.kr, idkim@kaist.ac.kr

Supporting Information

Table of Contents

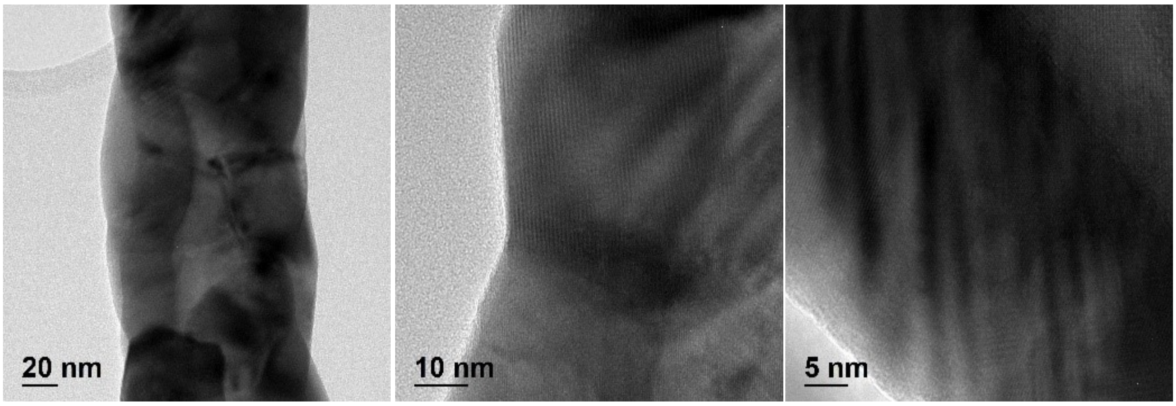

Figure S1. Additional TEM images of 0_$LaFeO_3$/SnO_2 NTs.

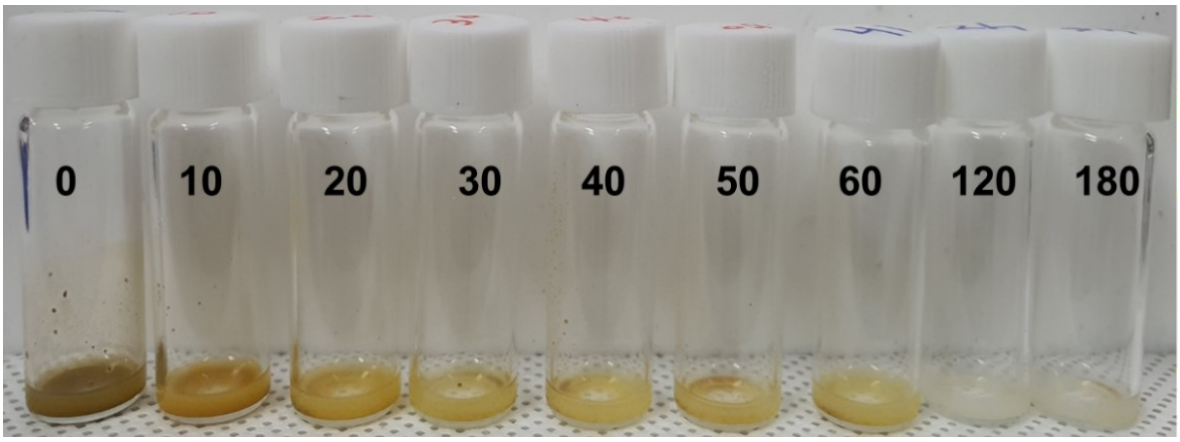

Figure S2. Digital camera images of suspension for gas sensing materials (unit; min).

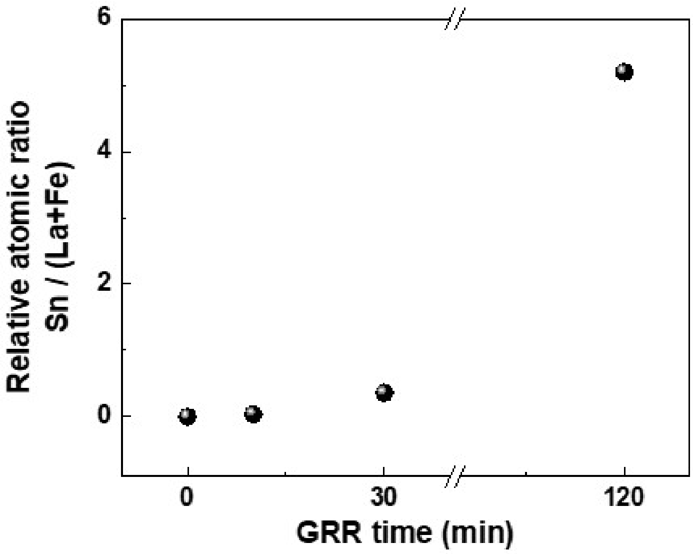

Figure S3. The relative atomic percent ratio of Sn to the sum of La and Fe as a function of GRR time (The values are determined by EDS mapping).

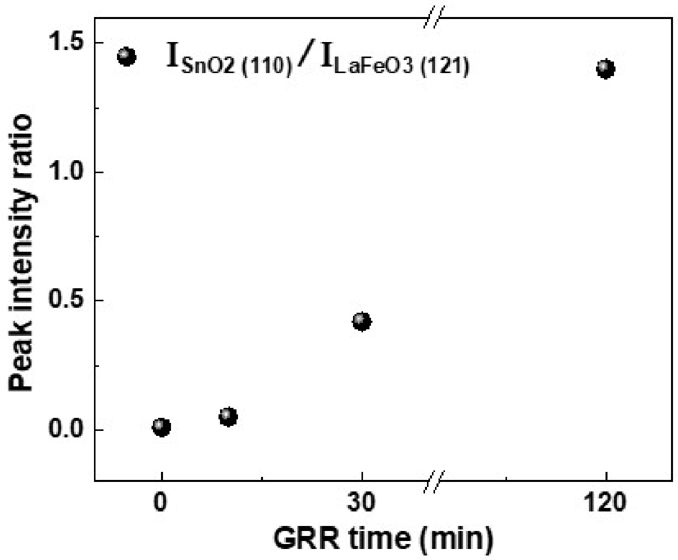

Figure S4. XRD patterns and relative peak intensities ratio of SnO_2 (110) to $LaFeO_3$ (121).

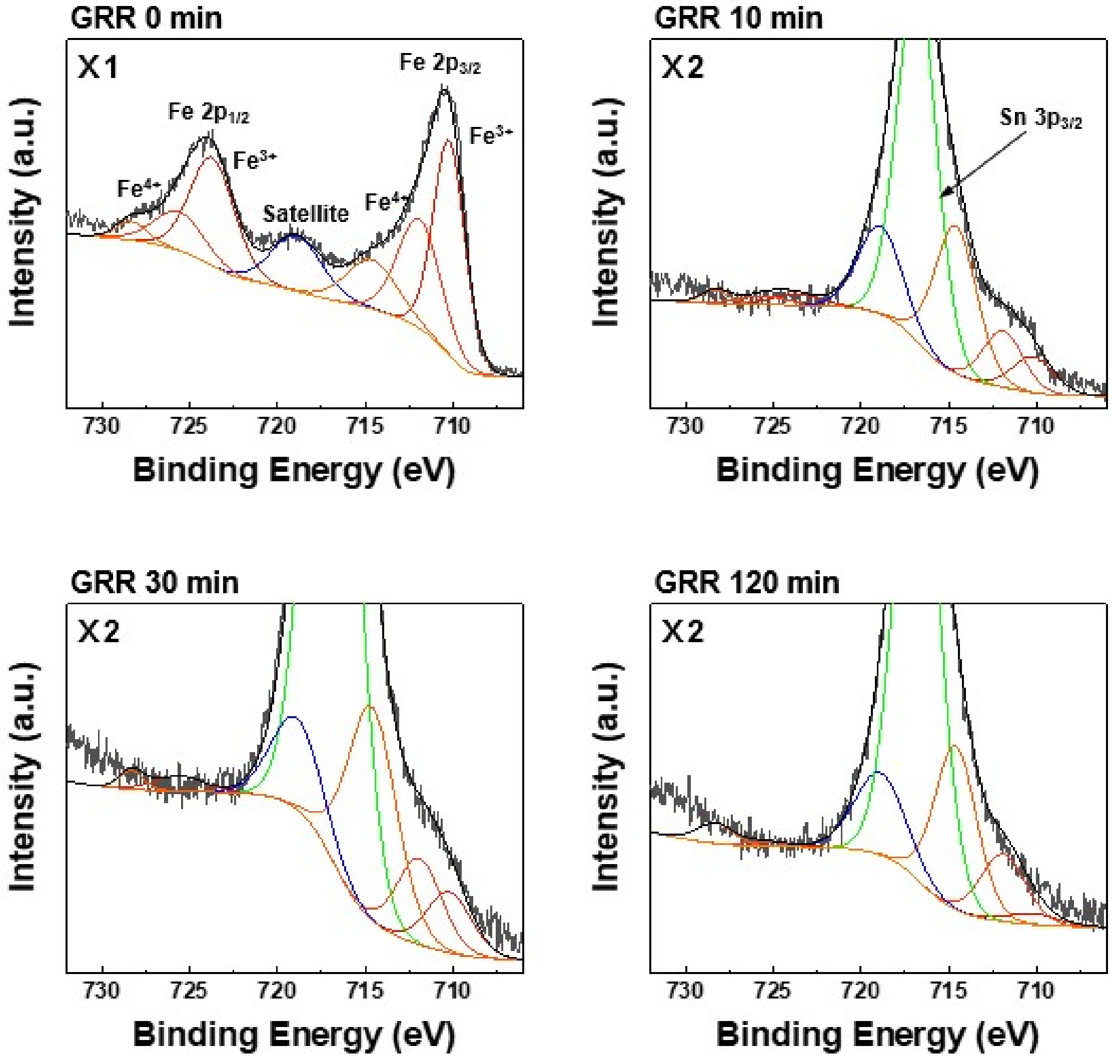

Figure S5. *Ex-situ* XPS spectra of Fe 2p in 0, 10, 30 and 120_$LaFeO_3/SnO_2$ NTs.

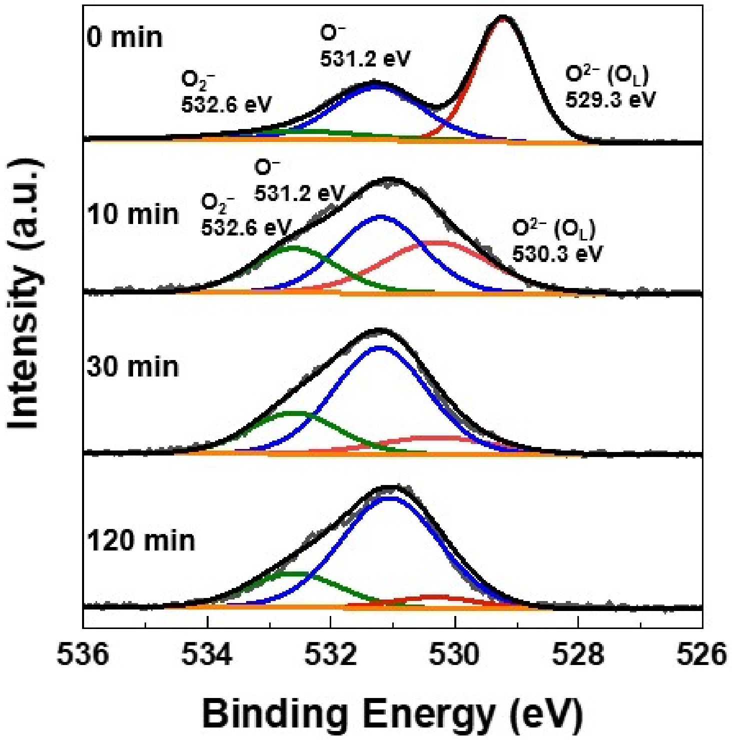

Figure S6. *Ex-situ* XPS spectra of O 1s in 0, 10, 30 and 120_$LaFeO_3/SnO_2$ NTs.

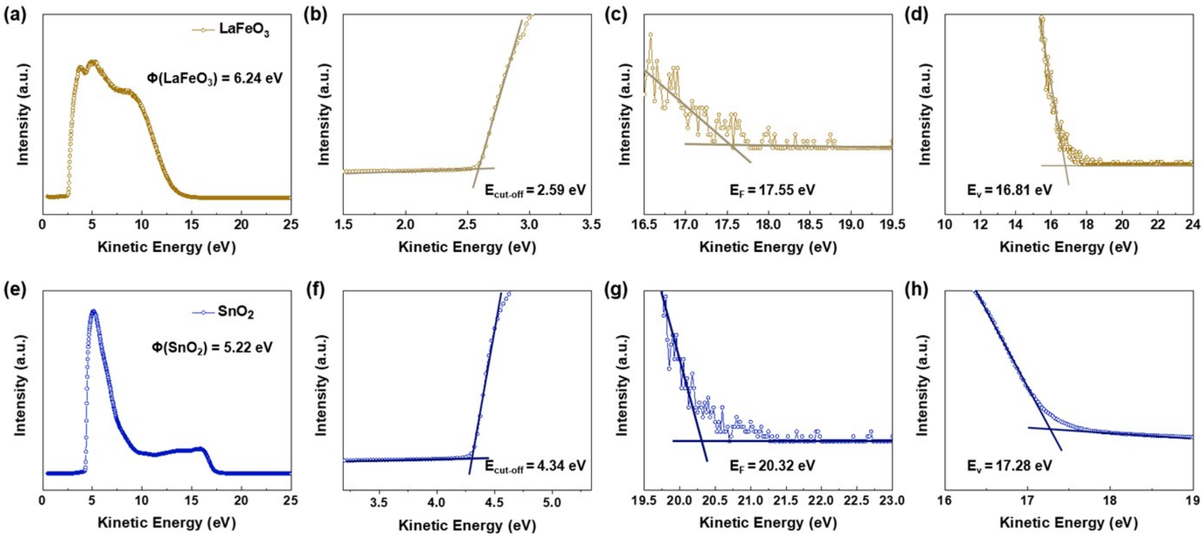

Figure S7. UPS spectra of (a-d) $LaFeO_3$, and (e-h) SnO_2.

A He-lamp with 21.2 eV (UV excitation by He I) excitation energy was used for the UPS analysis and the work function of samples was calculated using the following equation (1).

$$\Phi \text{ (work function)} = h\nu \text{ (He I line, 21.2 eV)} - |E_{cut\text{-}off} - E_f| \quad (1)$$

Based on UPS results, the derived work functions of the $LaFeO_3$ and SnO_2 were 6.24 eV, and 5.22 eV, respectively.

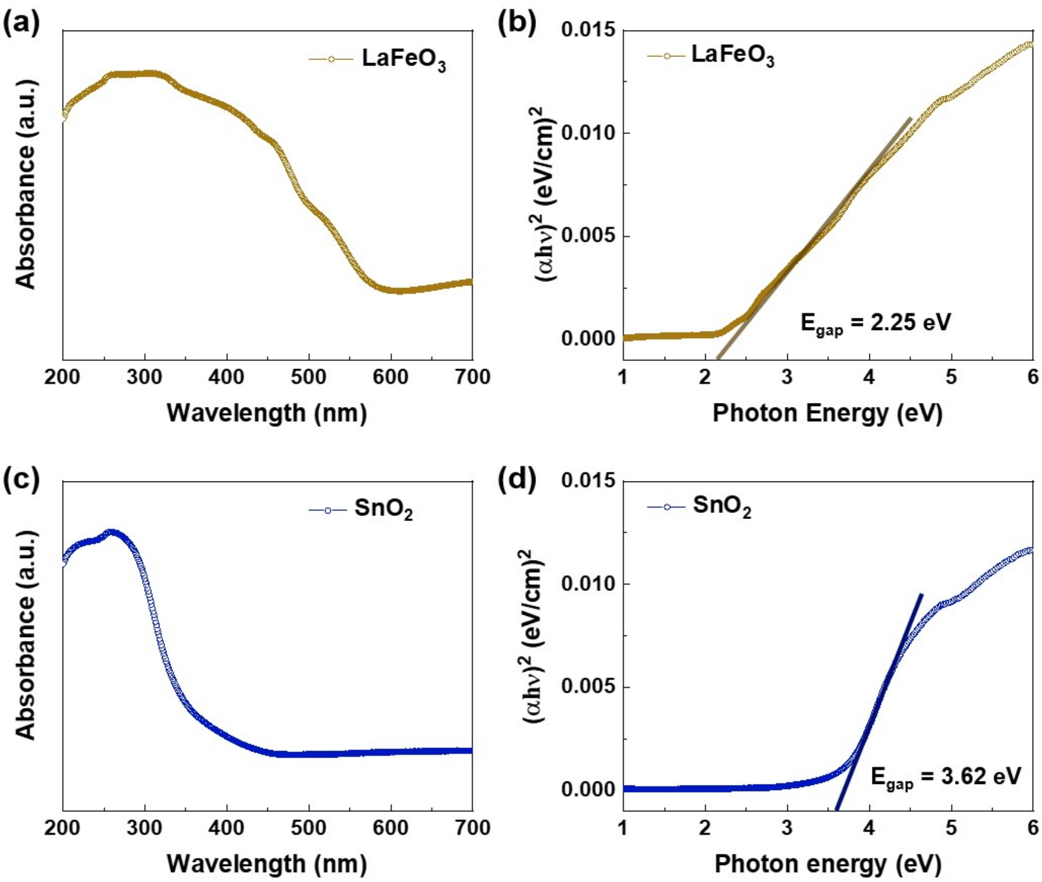

Figure S8. UV-VIS absorbance spectra, and Tauc plots of (a-b) $LaFeO_3$, and (c-d) SnO_2 samples.

The estimated band gap energy of $LaFeO_3$ was 2.25 eV, while the band gap energy of the SnO_2 was 3.62 eV.

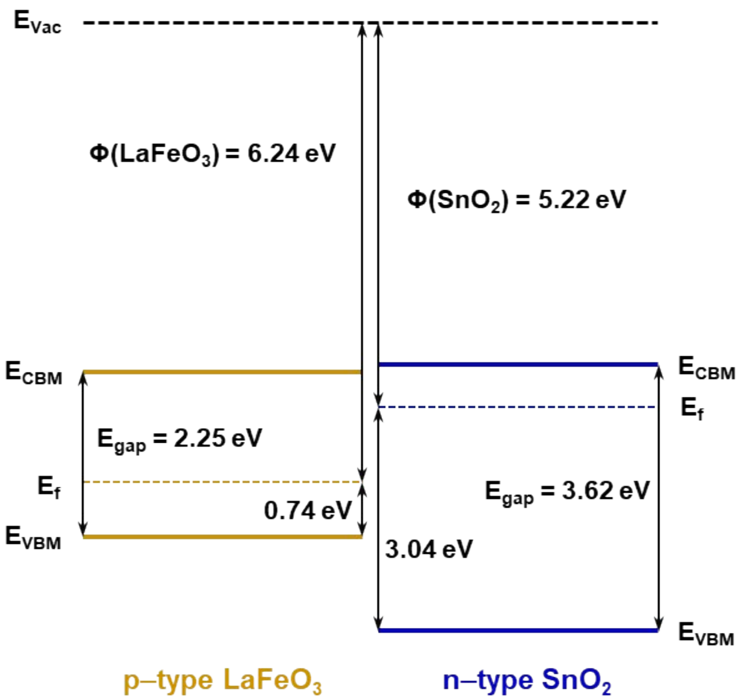

Figure S9. Simplified energy band diagram of the $LaFeO_3$ and SnO_2.

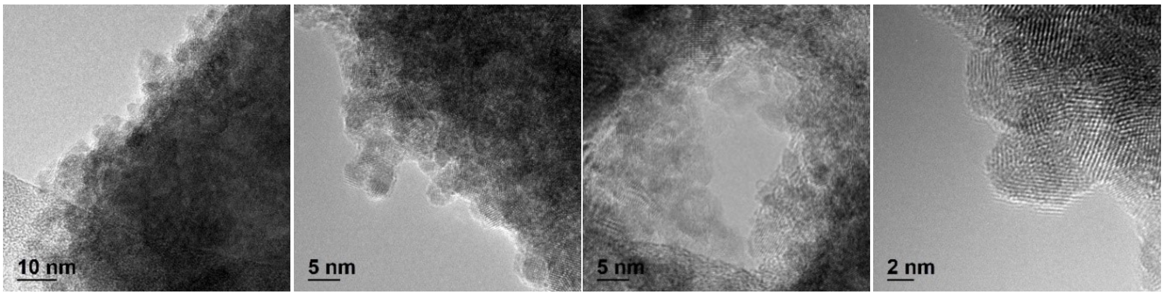

Figure S10. Additional TEM images of 30_$LaFeO_3$/SnO_2 NTs.

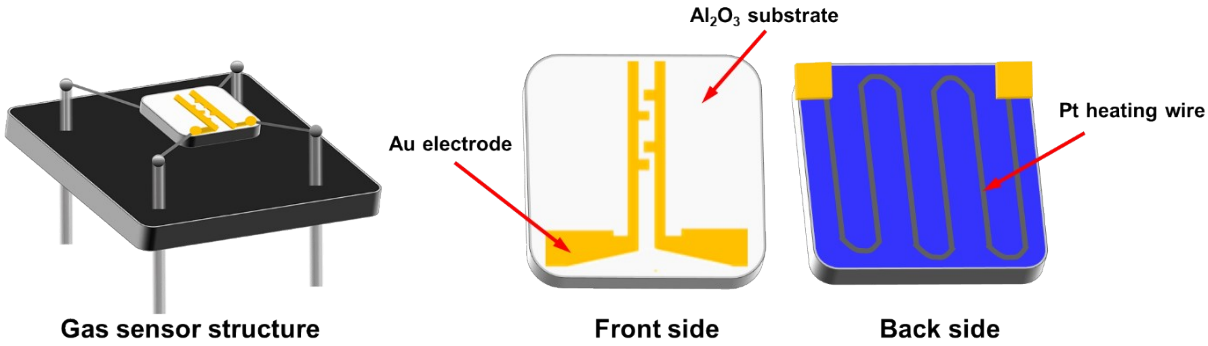

Figure S11. Schematic illustrations of the gas sensor structure.

The sensor substrates have three main components: an alumina board support, printed Au electrodes, and Pt heating wires. The size of the alumina support is 2.5 mm x 2.5 mm (thickness: 0.2 mm), and the substrates were printed on one side with a pair of interdigitated Au electrodes (width: 25 μm, distance: 70 μm) and decorated with a Pt heating wire on the other side. The alumina support is connected to the four-pin systems with Pt wires. The connected two pins of electrodes measured resistance between electrodes, and the other pins were connected to the Pt heater, which measured the operating temperature.

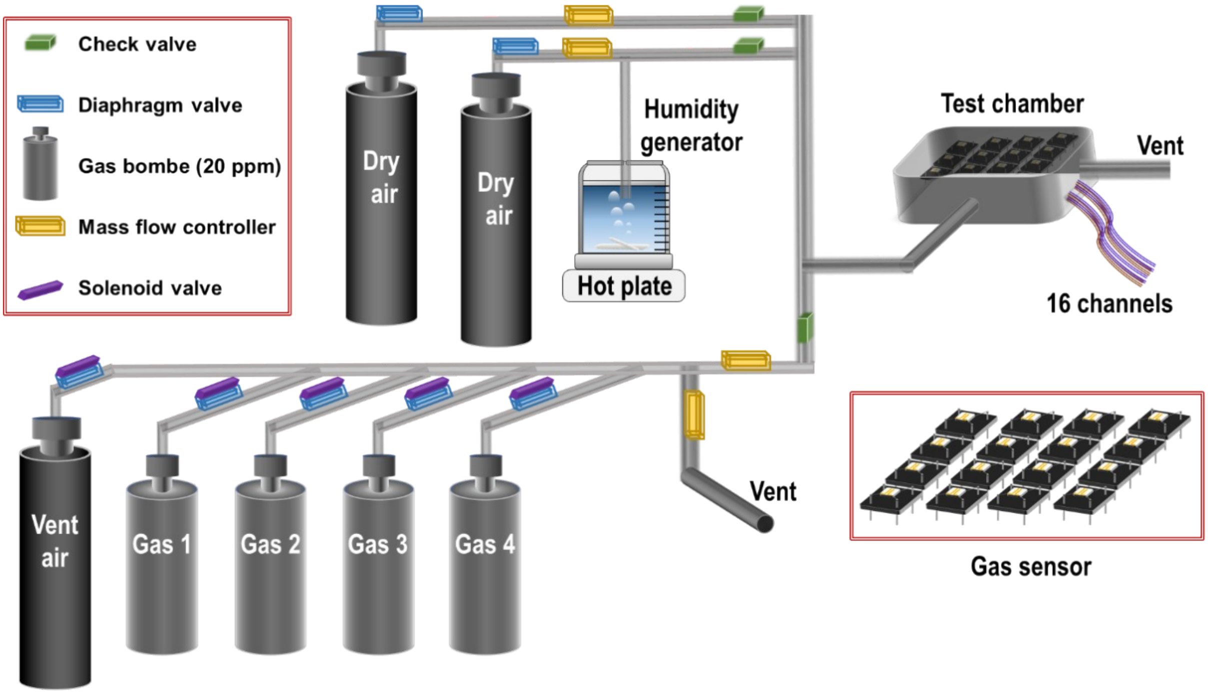

Figure S12. Schematic illustrations of the gas sensor measurement system.

The gas sensing tests were operated using a home-made gas sensing system consisting of a 16-channel multiplexer (34902A, Agilent) equipped with a data acquisition system (34972A, Agilent) for measuring the resistance of sensors through 16 channels at 4-s intervals, as well as a mass flow control system for controlling the concentration of exposed gases. The sensing measurements were operated in a highly humid atmosphere (90% RH), which is similar to the conditions in exhaled breaths of humans. The operating temperatures were controlled by applying a voltage to the Pt microheaters in the sensor substrate using a DC power supply (E3647A, Agilent).

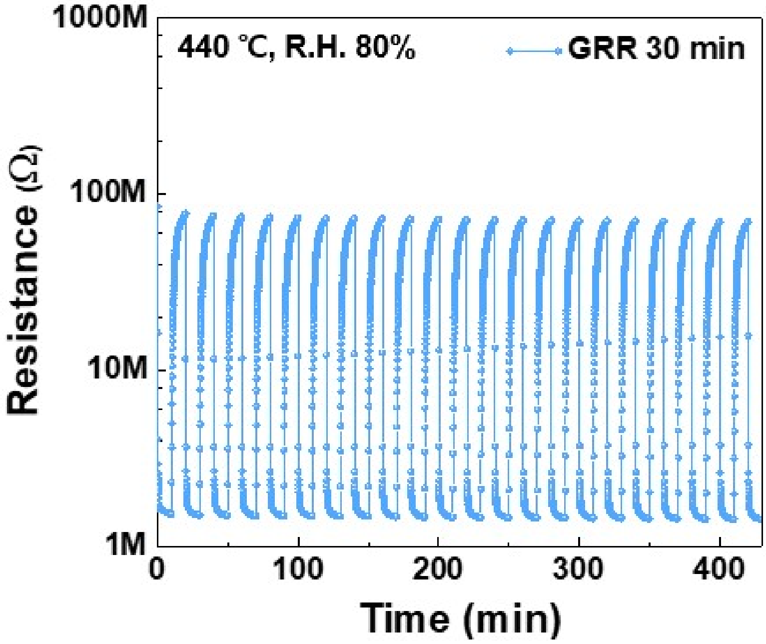

Figure S13. Reliability tests using 30_$LaFeO_3$/SnO_2 sensors upon 21 cyclic exposures to 5 ppm C_2H_2.

Table S1. Average grain sizes of $LaFeO_3/SnO_2$ NTs calculated by Scherrer equation.

	$LaFeO_3$	SnO_2
0_$LaFeO_3/SnO_2$ NTs	39.7 nm	–
30_$LaFeO_3/SnO_2$ NTs	44.7 nm	3.0 nm

Scherrer equation is known as follows:

$$d = \frac{0.9\lambda}{\beta cos\theta}$$

Where, d is the average crystallite size

λ, Wavelength of the X-ray is 0.154 nm

θ, Bragg diffraction angle

β, Full width at half maximum intensity (FWHM)

Peaks at $2\theta = 32.2° \pm 0.1°$ and 26.7° were selected to estimate the grain size of $LaFeO_3$ and SnO_2 from 0 and 30_$LaFeO_3/SnO_2$ NTs, respectively. The values were taken from the XRD results in Figure 3a.

Table S2. The proportion of oxygen species and relative ratios (O^-/O^{2-}). The values were taken from the *Ex-situ* XPS spectra of O 1s in Fig. S6.

Proportion of peak area (%)	O_2^-	O^-	O^{2-}	O^-/O^{2-}
0_$LaFeO_3/SnO_2$ NTs	9.2	36.8	54.1	0.7
10_$LaFeO_3/SnO_2$ NTs	24.6	41.0	34.4	1.2
30_$LaFeO_3/SnO_2$ NTs	23.1	64.1	12.8	5.0
120_$LaFeO_3/SnO_2$ NTs	21.0	72.5	6.5	11.1